1. Michał STYŁA[1], 2. Dominik GNAŚ[2], 3. Przemysław ADAMKIEWICZ[1,2]

Information Technology Research & Development Centre (CBRTI sp. z o. o.), Rzeszów (1), WSEI University, Lublin (2)
ORCID: 1. 0000-0002-1141-0887; 2. 0000-0002-8169-9700; 3. 0000-0003-3425-9566

doi:10.15199/48.2025.02.04

Implementation of reflective methods for microwave frequency signal processing in radio tomography

Abstract. *The project consisted in the application of electromagnetic waves in the 5.8 GHz band and radio tomography technology to detect the occupants, using reflective methods. The employed activities included the creation of a concept for the hardware layer, the structure and hierarchy of the data transfer network, as well as a method for processing the acquired waveforms into useful information. An additional advantage was to be the combination of analysis of signatures obtained by reflection with transmission tomography at 2.4 GHz.*

Streszczenie. *Projekt polegał na wykorzystaniu fal elektromagnetycznych w paśmie 5,8 GHz oraz technologii tomografii radiowej do wykrywania osób przebywających w pomieszczeniach przy użyciu metod refleksyjnych. Działania obejmowały stworzenie koncepcji warstwy sprzętowej, struktury i hierarchii sieci transferu danych, a także metody przetwarzania pozyskanych przebiegów na użyteczne informacje. Dodatkowym atutem miało być połączenie analizy sygnatur otrzymywanych drogą odbiciową z tomografią transmisyjną na częstotliwości 2,4 GHz* ***(Implementacja metod refleksyjnych do przetwarzania sygnałów o częstotliwości mikrofalowej w tomografii radiowej)***

Keywords: radiolocation techniques; radio tomography; indoor navigation; device-free localization.
Słowa kluczowe: techniki radiolokacyjne; tomografia radiowa; nawigacja wewnątrzbudynkowa; lokalizacja bez urządzeń.

Introduction

The presented radio tomography system is aimed at building objects requiring a higher degree of targeting precision than other transmission methods of radio signal processing [1-8]. It is an original hardware and software solution, the description of which contained in this paper is both a characterization of the electronic components used in its construction and of the computational algorithms unsupported and supported by machine learning mechanisms [9-13]. There are many methods for analyzing and reconstructing measurement data [14-20]. The system's primary task in question is to locate users indoors using a hybrid tracking method based on radio transmission tomography and radio reflection tomography.

Design of the device

The focal point of the device is the MAX2828ETN+ transceiver, which is a front-end system, i.e. without an internal control unit in the form of a microcontroller, but controlled externally by means of registers and the bit/flag values contained therein. The transmit and receive paths are separated from each other and independently controlled. The master control functions are provided by a WSoC (Wireless System on a Chip) nRF52832 microcontroller. It performs the additional function of transporting readings from environmental sensors via Bluetooth 5. The rest of the components used are complex HF filtering and conditioning circuits and integrated reference signal sources for timing or synthesis of other signals. The carrier frequency signal can be derived and fed into the circuit via a quad-patch microwave antenna, which is attached to the PCB via an SMA connector or by a 'sandwich' method with the help of spacers via special transceiver line terminations. The final device parameters settled on a laminate with a size of 106 x 80 x 1.6 mm, radiated power of 10 mW, and an effective range of 10 meters. The board has been fabricated on a standard 1.6mm thick FR4 dual-layer laminate. The top and bottom copper layers have a thickness corresponding to a value of one ounce (1 oz.). To minimize the risk of the conductor's sharp edges adversely affecting the performance of the radio circuits, all signal connections and the copper spout have been rounded off. Potentials between the top and bottom layers were equalized using regularly spaced vias. The radio signal lines have been shielded along the entire length of the transmission line and the areas immediately adjacent to the transmit and receive antennas have been completely free of ground polygons. The device's final appearance is shown in Figures 1, 2 and 3.

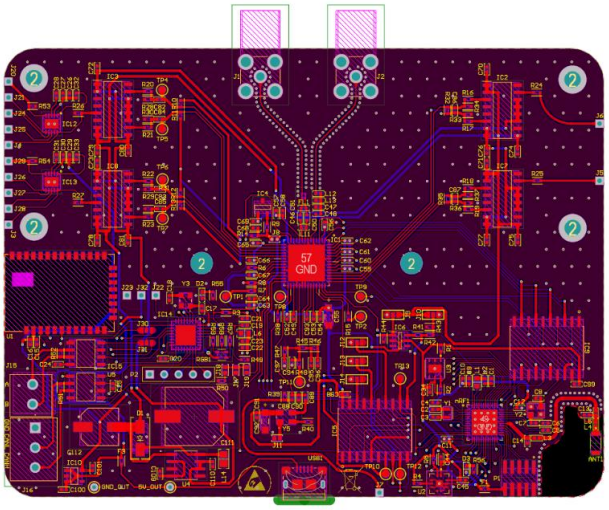

Fig. 1. Radio reflection probe prototype – a patchwork of electrical connections

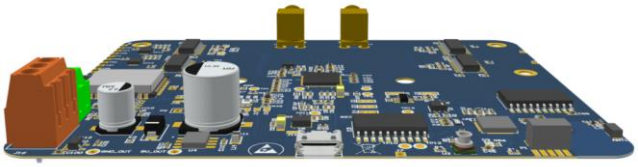

Fig. 2. 3D visualization of the printed circuit board of a hybrid tomographic probe

The hardware solution consists of a radio probe using frequencies in the 2.4 GHz band using an nRF52832 or EM357 microcontroller (transmission tomography) and 10.5 GHz using a microwave oscillator (reflection tomography). In addition to the antenna paths and frequency sources, the platform was equipped with a number of passive filters, broadband amplifiers and the signal sources needed for synthesis. An STM32 F3-series microcontroller coordinates the two parts of the tomograph, while a CAN bus controller carries the data it receives to the computing cluster. The data transported via CAN reaches a central unit wired to the

local network. The final step is to create a complete data set from the received data and then output it in JSON format to the Apache Kafka data bus.

Based on the signals read from the sensors of the 32 sensors (16 sensors are placed at a height of 1.2 m from the floor and 16 sensors are placed at a height of 1.55 m from the floor), a visualization of the viewing area is made. A reconstruction is made for each ring, where the main problem is to recognize the number of inclusions and then present the reconstruction for each ring separately and the reconstruction in 3D space. An example of a system installation view is shown in Figure 4.

Fig. 3. Radio reflection probe prototype – genuine specimen

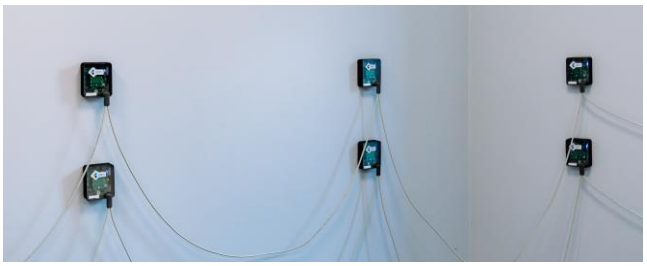

Fig. 4. Two hybrid probe measurement rings installed in the test room

The sequencing of data acquisition from the measurement rings was realized by a central unit imposing a selected radio probe to transmit samples while the measurement was performed independently and cyclically. This approach allowed even greater control over data integrity. A refresh rate of 2 full frames per second allows, to some extent, the retransmission to be included in the measurement algorithm without having to supplement the data with samples from the preceding set. The CAN bus speed has been set to 1 Mbit/s and is not adjustable, but the probe's speed as an independent unit can be adjusted over a wide range using a dedicated API. Parameters such as the number of queries per second, the method and number of samples when averaging the result, or the signal gain for the microwave emitter and detector can be modified.

The advantage of such a solution is the high flexibility in scaling up the system due to the various building rooms. This applies both to the speed of operation of the individual system blocks, which directly impacts energy efficiency, and to the number of devices for optimal grid distribution for transmission tomography, as well as the operating range and viewing angles of the microwave detectors.

Signal processing and reconstruction procedures

The user's position information was determined from a transmitter network of 16 reflection probes in a room-bound arrangement, characteristic of tomography. Waves reflected from objects returning to the detector were amplified and filtered, then passed to a circuit that reduced their frequency so that the ADC could successfully sample them. A CAN bus and an access gateway with access to the building's local network were responsible for transporting the data to the location engine located on the computing server. Each packet containing a signal sample was equipped with probe number information and a time stamp to maintain the synchronization/consistency of the data sets. Example visualizations obtained from the amplitude and frequency analysis of the signals are presented in Figure 5. One starting point for the signal processing was to relate the amplitude to the distance from the detector/presence at the detector, and the other was to use the Doppler phenomenon for object movement. Extreme unfavorable cases of movement parallel to the detector were counterbalanced by readings from other probes where the movement shown was more unambiguous. The disappearance of motion below a certain threshold caused the last known position of the object to be remembered and resumed when the oscillograms fluctuated again. The maximum response from the reflection probes was induced within the radiation pattern of their microwave antennas, i.e. 45 degrees horizontally and 30 degrees vertically, resulting in a final accuracy of 40 to 50 cm, depending on the prevailing conditions.

The following description outlines the methodology leading to the 2D reconstruction. The viewing area consists of 2437 finite elements. The 2D visualization algorithm was made as follows:

1. visual area reconstruction imaging;
2. conversion of the image to greyscale;
3. determination of greyscale pores and cut-off;
4. elimination of artifacts (very small inclusions/holes);
5. determination of clusters and cluster centroids.

For reconstruction and visualization, the following functions have been defined: one to detect the number of objects and the other to visualize inclusions in the viewing area. These two activities were used for both rings. This further determines inclusion imaging in 3D visualization.

The result of the algorithm and the visualization of the recognition of the number of objects is presented below. Under each graph, additionally, the values of the inclusion coordinates (marked with a red point on the graphs) and the number of objects recognized by the algorithm are given. A model based on the gradient boosting classifier was created for each finite element. Based on this, we estimate the probability that a finite element belongs to the inclusion area. Reconstruction involves identifying areas containing finite elements that have probabilities above a fixed threshold. These areas correspond to the position of people in the room. The image reconstructions are presented in Figure 6.

The following descriptions outline the methodologies leading to the 2.5D and 3D reconstruction. 2.5D visualization algorithm was made as follows:

1. creation of a 2D mesh for each level;

2. assignment of values for the pixels that are closest to the finite elements for a ring at a distance of 1.2m from the floor;
3. assignment of values for the pixels that are closest to the finite elements for the ring at a distance of 1.55m from the floor;
4. 3D visualization for each level.

The 3D visualization algorithm was made as follows:

1. creation of a 3D mesh;
2. assignment of values for the voxels that are closest to the finite elements for the ring at a distance of 1.2m from the floor;
3. assignment of values for the voxels that are closest to the finite elements for the ring at a distance of 1.55m from the floor;
4. visualizing the space between 1.2m and 1.55m from the floor in 3D.

The functions for the reconstruction of the viewing area 2.5D and 3D were created for the visualization. Below are the results of the 2.5D visualization (where different colors at different levels represent the inclusion areas, the expected time of determining the inclusions with presentation is about 0.1 seconds) and the results of the 3D visualization (we approximate the inclusions body additionally between the two rings which located at heights of 1.2 m and 1.55 m from the room floor, then the expected time of visualization elongates to 1 second). The image reconstructions for the multivariate analysis are presented in Figures 7 and 8.

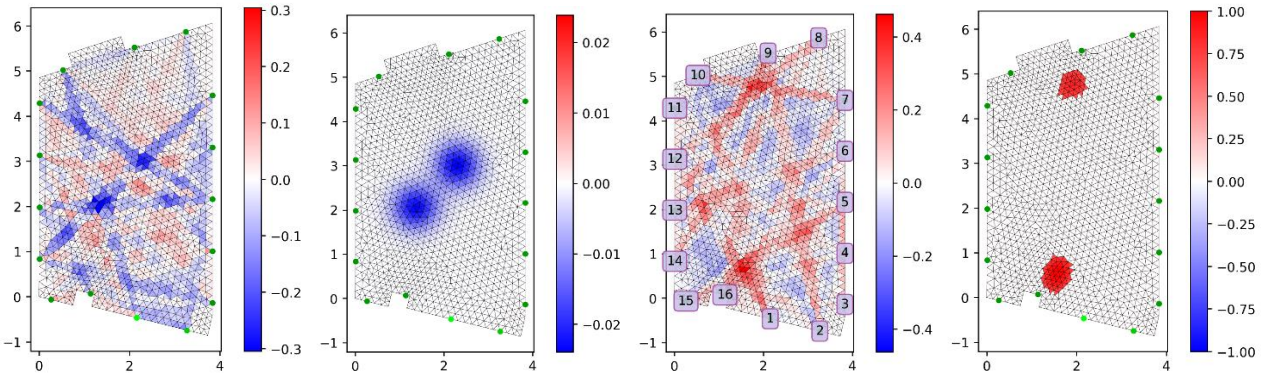

(a) (b) (c) (d)

Fig. 5. Visualisation of users positions based on amplitude and frequency analysis of waveforms (relative units): (a) – TSVD direct result (static scenario I), (b) – direct TSVD result with Gaussian filtration (static scenario I), (c) – TSVD direct result (static scenario II), (d) – direct TSVD result with Mexican Hat filtration (static scenario II)

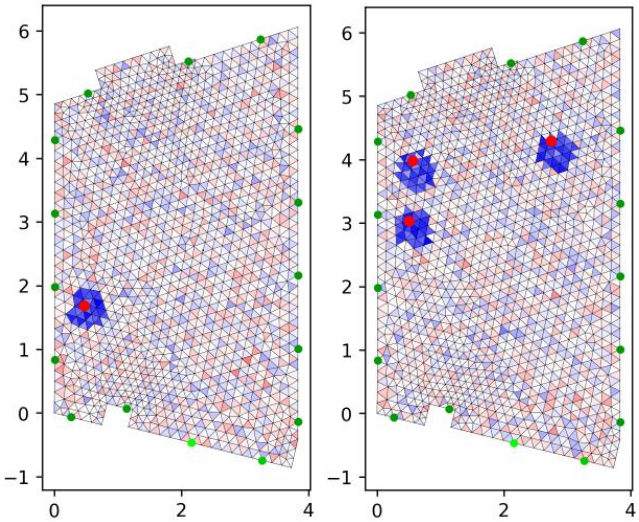

Fig. 6. Presentation method for 2D visualization (single object - left and multiple objects - right)

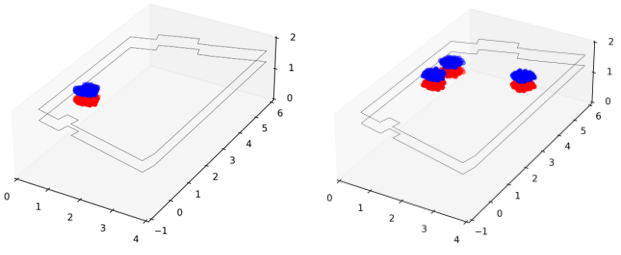

Fig. 7. Image reconstructions for multivariate analysis – summary of readings from both measuring rings

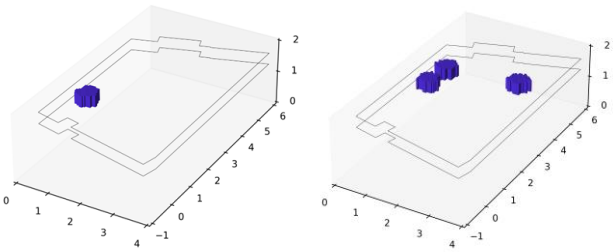

Fig. 8. Image reconstructions for multivariate analysis – the final form

Results and conclusions

The method used for reconstruction accurately reflects the position of people/objects in the room presented. In the case of layered 2.5D imaging, the time needed to complete reconstruction is about 0.1 seconds, while in the case of 3D reconstruction with approximation between rings, the time is getting longer. The solution can be used for navigation systems and localization technology installed in buildings. In addition, this approach can reduce building maintenance costs (the lights turn off when they detect that there are no people in the room or corridor).

***Authors**: Michał Styła, MSc., Information Technology Research & Development Centre (CBRTI sp. z o. o.), Rzeszów, Poland, E-mail: michal.styla@cbrti.pl; Dominik Gnaś, MSc., Information Technology Research & Development Centre (CBRTI sp. z o. o.), Rzeszów, Poland, E-mail: dominik.gnas@cbrti.pl; Przemysław Adamkiewicz, Ph.D., Information Technology Research & Development Centre (CBRTI sp. z o. o.), Rzeszów, Poland, WSEI University, Lublin, Poland, E-mail: przemyslaw.adamkiewicz@cbrti.pl.*

REFERENCES

[1] Brodeski, D., Bilik, I., Giryes, R. Deep Radar Detector, *2019 IEEE Radar Conference (RadarConf)*, 22–26 April 2019

[2] Wnuk M., Chudy, Z. Pomiar mocy impulsu elektromagnetycznego mikrofal, *Przegląd Elektrotechniczny*, 90 (2014), No. 8, 239–242

[3] Bilik, I., Bialer, O., Villeval, S., Sharifi, H., Kona, K., Pan, M., Persechini, D., Musni, M., Geary, K. Automotive MIMO radar for urban environments, *2016 IEEE Radar Conference (RadarConf)*, 02–06 May 2016

[4] Zhang, C., Luo, W., Urtasun, R. Efficient Convolutions for Real-Time Semantic Segmentation of 3D Point Clouds, *In Proc. International Conference on 3D Vision (3DV*), 2018

[5] Styła, M., Kiczek, B., Kłosowski, G., Rymarczyk, T., Adamkiewicz, P., Wójcik, D., Cieplak, T. Machine Learning-Enhanced Radio Tomographic Device for Energy Optimization in Smart Buildings, *Energies*, 16 (2022), No. 1, 275

[6] Yadav, R., Omrani, A., Link, G., Vauhkonen, M., Lähivaara, T. Microwave Tomography Using Neural Networks for Its Application in an Industrial Microwave Drying System, *Sensors*, 21 (2021), No.20, 6919

[7] Yuchong. Z., Yong, Ma., Ormani, A., Rahul, Y., Morten F., Marco, F. Automated Microwave Tomography (MWT) Image Segmentation: State-of-the-Art Implementation and Evaluation, *WSCG 2020: Full Papers Proceedings, Václav Skala - UNION Agency*, 126 – 136, 2020

[8] Kłosowski G, Rymarczyk T, Niderla K, Kulisz M, Skowron Ł, Soleimani M. Using an LSTM network to monitor industrial reactors using electrical capacitance and impedance tomography – a hybrid approach, *Eksploatacja i Niezawodnosc – Maintenance and Reliability*, 25 (2023). No.1

[9] Rybak G, Kozłowski E, Król K, Rymarczyk T, Sulimierska A, Dmowski A, Bednarczuk P. Algorithms for Optimizing Energy Consumption for Fermentation Processes in Biogas Production*. Energies,* 16 (2023), No. 24, 7972

[10] Styła M., Kozłowski E., Tchórzewski, P., Gnaś, D., Adamkiewicz, P., Laskowski, J., Skrzypek-Ahmed, S., Małek, A., Kasperek, D. Detection and Determination of User Position Using Radio Tomography with Optimal Energy Consumption of Measuring Devices in Smart Buildings, *Energies*, 17 (2024), No.11, 2757

[11] Dubey, A., Sood, P., Santos, J., Ma, D., Chiu, C., Murch, R. An Enhanced Approach to Imaging the Indoor Environment Using WiFi RSSI Measurements, *IEEE Transactions on Vehicular Technology*, 70 (2021), No.9, 8415 – 8430

[12] Wei, Z., Zhang, F., Chang, S., Liu, Y., Wu, H., Feng, Z. MmWave Radar and Vision Fusion for Object Detection in Autonomous Driving: A Review, *Sensors*, 22 (2022), No.7, 2542

[13] Chen, X., Su, N., Huang, Y., Guan, J., False-Alarm-Controllable Radar Detection for Marine Target Based on Multi Features Fusion via CNNs, *IEEE Sensors Journal*, 21 (2021), No.7, 9099 – 9111

[14] Baran B, Kozłowski E, Majerek D, Rymarczyk T, Soleimani M, Wójcik D. Application of Machine Learning Algorithms to the Discretization Problem in Wearable Electrical Tomography Imaging for Bladder Tracking*, Sensors,* 23 (2023), No. 3,1553

[15] Przysucha B, Wójcik D, Rymarczyk T, Król K, Kozłowski E, Gąsior M. Analysis of Reconstruction Energy Efficiency in EIT and ECT 3D Tomography Based on Elastic Net*, Energies,* 16 (2023), No. 3, 1490

[16] Kozłowski E., Borucka A., Oleszczuk P., Jałowiec T., Evaluation of the maintenance system readiness using the semi-Markov model taking into account hidden factors, *Eksploatacja i Niezawodność – Maintenance and Reliability,* 25 (2023), No. 4, 172857

[17] Panskyi T, Korzeniewska E, Firych-Nowacka A. Educational Data Clustering in Secondary School Sensor-Based Engineering Courses Using Active Learning Approaches*. Applied Sciences,* 14 (2024), No.12, 5071

[18] Maciura, Łukasz, Wójcik, D., Rymarczyk, T., Król, K., Novel hybrid algorithm using convolutional autoencoder with SVM for electrical impedance tomography and ultrasound computed tomography. *Informatyka, Automatyka, Pomiary W Gospodarce I Ochronie Środowiska,* 13 (2023), No. 2, 4–9

[19] Kulisz M., Kłosowski G., Rymarczyk T., Hoła A., Niderla K., Sikora J., The use of the multi-sequential LSTM in electrical tomography for masonry wall moisture detection*, Measurement,* 234 (2024) 114860*.*

[20] Soleimani M., Rymarczyk T., Kłosowski G., Ultrasound Brain Tomography: Comparison of Deep Learning and Deterministic Methods*, IEEE Transactions on Instrumentation and Measurement,* 73 (2024), 4500812